Electronic Supplementary Information

Linker Engineering in Mixed-Ligand Metal-Organic Frameworks for Simultaneously Enhanced Benzene Adsorption and Benzene/ Cyclohexane Separation

Yong-Zheng Zhang,[a,b,†] Xin-Dan Zhang,[a,b,†] Yan-Kai Zhang,[a,b] Fu-Tian Wang,[a] Longlong Geng,[a,b,*] Hui Hu,[a] Zhen Li,[a] Da-Shuai Zhang,[a,b,*] Hongliang Huang,[c,*] Xiuling Zhang [a,b]

[a] *Shandong Provincial Key Laboratory of Monocrystalline Silicon Semiconductor Materials and Technology, Shandong Universities Engineering Research Center of Integrated Circuits Functional Materials and Expanded Applications, College of Chemistry and Chemical Engineering, Dezhou University, Dezhou 253023, P. R. China.*

[b.] *School of Chemistry and Chemical Engineering, Shandong University of Technology, Zibo 255000, China*

[c.] *State Key Laboratory of Separation Membranes and Membrane Processes, School of Chemical Engineering and Technology, Tiangong University, Tianjin 300387, China*

[†] *Yong-Zheng Zhang and Xin-Dan Zhang contributed equally to this work.*

***Corresponding author**

Longlong Geng, E-mail: llgeng@126.com

Da-Shuai Zhang, E-mail: dashuai_74@163.com

Hongliang Huang, E-mail: huanghongliang@tiangong.edu.cn

Section 1. Experimental

Materials and Methods

The TMTPB, H_2BDC, and H_2NDC ligands were acquired from Jilin Yanshen Technology Co., Ltd., Chinese Academy of Sciences. N,N-dimethylacetamide (DMA, 99.9%) and ethanol (EtOH, 99.7%) were sourced from China National Pharmaceutical Group Corporation. Hydrogen tetrafluoroborate (HBF_4, 50 wt% H_2O), Bz (99.5%), and Cy (99.5%) were purchased from Macklin Technology Co., Ltd. Methanol (Meth, 99.7%) was obtained from Kemio Chemical Reagent Co., Ltd. $Ni(NO_3)_2 \cdot 6H_2O$ was procured from Beijing Nuochuang Chemical Technology Co., Ltd. Powder X-ray diffraction (PXRD) data were collected using a Bruker D8 ADVANCE X-ray diffractometer with Cu K-α radiation (λ = 0.1542 nm), in the 2θ range of 5-50°, operating at 40 kV and 40 mA at room temperature. Fourier-transform infrared (FT-IR) spectra were measured using a Shimadzu FTIR-8400S spectrometer. Thermal gravimetric analysis (TGA) was conducted under a nitrogen atmosphere using a NETZSCH STA449 F5 thermal analyzer, with the temperature ramped from ambient to 800 °C at a rate of 10 °C per minute. The morphology and element composition were recorded by scanning electron microscopy (SEM, S-4800, Hitachi). Gas adsorption of N_2 is determined using a corrosive gas adsorption analyzer (BSD-PMC). Vapor adsorption tests of Bz and Cy were performed using a volumetric gas sorption analyzer (BSD-VVS) based on the multi-site adsorption method. The adsorption breakthrough test of Bz/Cy was conducted using a multi-component adsorption breakthrough curve analyzer (BSD-MAB). The content of Bz and Cy was analyzed using an online mass spectrum analyzer (INFICON).

Crystal Data Collection and Refinement

Single crystal X-ray diffraction (**SCXRD)** data for two crystal samples were collected using a Bruker diffractometer with the Mo-Kα radiation (λ = 0.71073 Å) at 150 K. Absorption correction was performed using the SADABS program.[S1] The structures were solved by the direct method and refined by full-matrix least-squares on F2 with

anisotropic displacement using the SHELXTL software package.[S2] The disordered C atoms in two MOFs were treated by occupancies refinement. Non-hydrogen atoms on the frameworks were refined with anisotropic displacement parameters during the final cycles. Hydrogen atoms of organic ligands were calculated in the ideal positions with isotropic displacement parameters, except those in the disordered atoms and coordinated μ_3-OH/H_2O groups. Although selected hydrogen atoms were not added but were calculated into molecular formula of the crystal data. For all MOFs, the volume fractions of disordered solvents in pores could not be modeled in terms of atomic sites, but were treated by using the MASK routine in the Olex2 software package.[S3] Crystal data can be found in Table S1.

Section 2. Calculation Procedures of Selectivity from IAST

The selectivity for the adsorbate mixture composition of interest was calculated from the single component adsorption isotherms using Ideal Adsorbed Solution Theory (IAST).[S4] First, single-component adsorption isotherm for each gas at 298 K was fitted with the single-site Langmuir-Freundlich equation (Equation S1).

$$N = A\frac{bp^c}{1 + bp^c} \quad \text{.....Equation S1}$$

In Equation S1, N is the adsorbed amount per mass of adsorbent (mmol g^{-1}), p is the pressure of the bulk gas at equilibrium with the adsorbed phase (kPa), A is the saturation capacities of sites A (mmol g^{-1}), b is the affinity coefficients of sites A (1/kPa), c represents the deviations from an ideal homogeneous surface. The fitting parameters of the Equation S1 for Bz and Cy are listed in the lower right table of the picture (Figure S9).

Second, based on the Equation S1 parameters of pure gas adsorption, we used the IAST model to investigate the separation of Bz/Cy in two MOFs, and the adsorption selectivity is defined by Equation S2:

$$S_{A/B} = \frac{x_A/y_A}{x_B/y_B}$$ .....Equation S2

Where S is the selectivity of component, A relative to B. x_A and x_B are the molar fractions of components A and B in the adsorption phase, respectively. y_A and y_B are molar fractions of components A and B in the gas phase, respectively.

Section 3. Computational Details

DFT calculations were carried out using the CP2K code.[S5] A mixed Gaussian and planewave basis sets were employed to the calculations. Core electrons were represented with norm-conserving Goedecker-Teter-Hutter pseudopotentials,[S6-8] and the valence electron wavefunction was expanded in a double-zeta basis set with polarization functions [S9] along with an auxiliary plane wave basis set with an energy cutoff of 400 eV. The generalized gradient approximation exchange-correlation functional of Perdew, Burke, and Enzerhof (PBE) [S10] was used. Each configuration was optimized with the Broyden-Fletcher-Goldfarb-Shanno (BGFS) algorithm with SCF convergence criteria of 1.0×10^{-8} au. To compensate the long-range van der Waals dispersion interaction between the adsorbate and the DZU-72 -73, the DFT-D3 scheme [S11] with an empirical damped potential term was added into the energies obtained from exchange-correlation functional in all calculations. Notably, the three-dimensional sizes and kinetic diameters of Bz and Cy are as follows: Bz is 3.3×6.6×7.3 Å³ and 5.85 Å, and Cy is 5.0×6.6×7.2 Å³ and 6.0 Å, respectively.[43,44] In DZU-72 and DZU-73, there are two types of cage structures, both sharing similar windows. As depicted in Fig. S14, the pore window size of cage B in DZU-72 is 5.2×5.2×8.9 Å³, while in DZU-73, it was measured to be 7.4×7.4×8.9 Å³. These dimensions suggest that the pore windows could accommodate the kinetic diameter of Bz more effectively than that of Cy, thus influencing the adsorption selectivity.

Independent gradient model (IGM) analyses were adopted to visually understand the noncovalent interactions and the atomic contributions for the host-guest

interaction.[S12] In this work, IGA analyses were based on the DFT calculated analyte adsorption configurations in DZU-72 and -73. The IGM analyses were achieved by Multiwfn software package 3.6,[S13] while the VMD 1.9.3 program [S14] was used to render the IGM visualized isosurface of weak interaction and atomic contributions for the host-guest interaction.

Section 4. Additional Figures

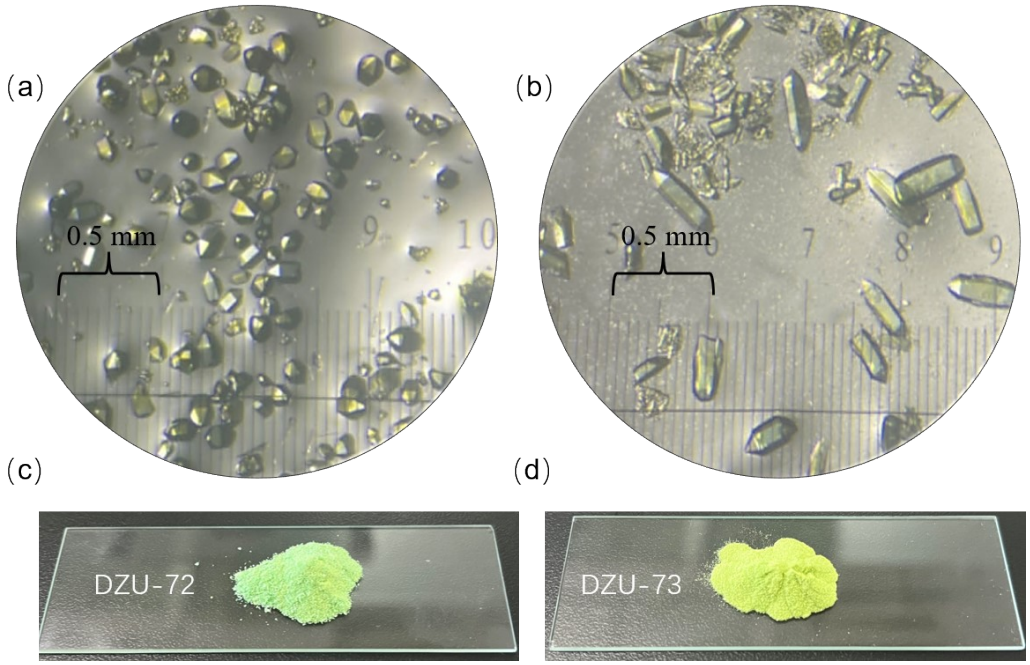

Fig. S1. Single crystal optical images of (a) DZU-72 and (b) DZU-73. Photograph showing the microcrystalline powder of three scaled-up two MOFs (c) DZU-72, and (d) DZU-73.

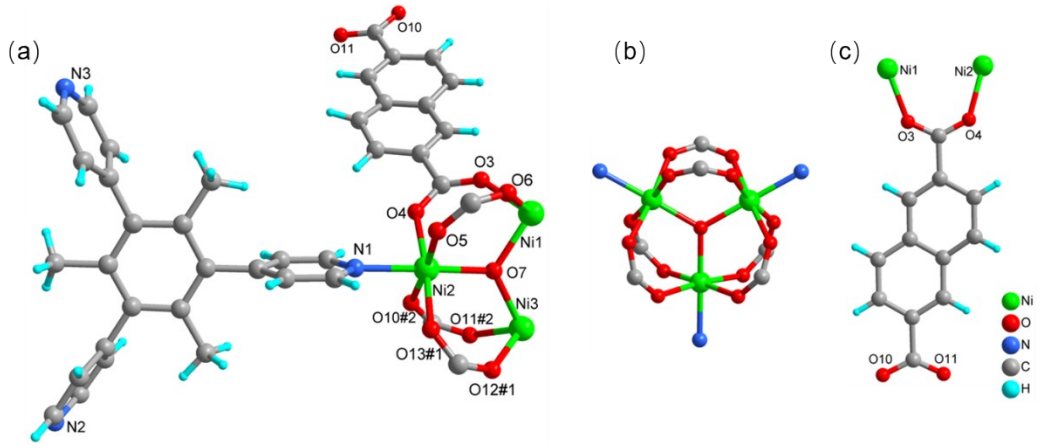

Fig. S2. (a) Coordination environment diagram of Ni(II) in DZU-73. (b) Trinuclear metal clusters.(c) Coordination mode diagram of NDC^{2-} ligand.

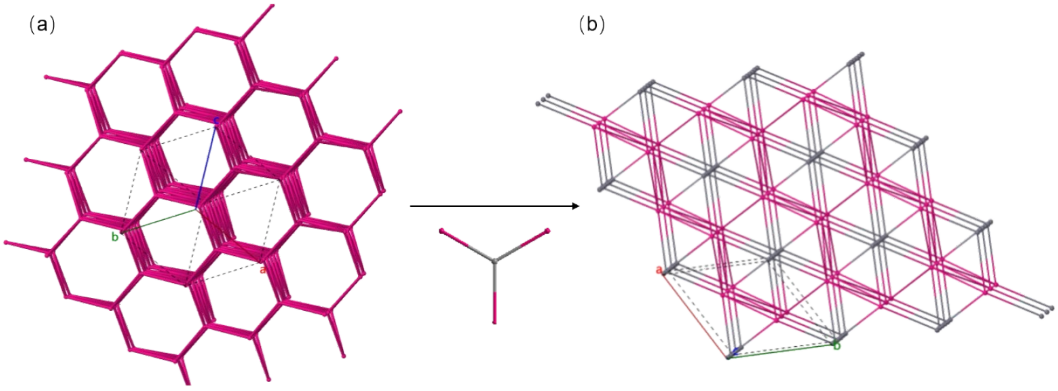

Fig. S3. The acs topology of MIL-88 (a) and the nia-d topology of DZU-73 (b).

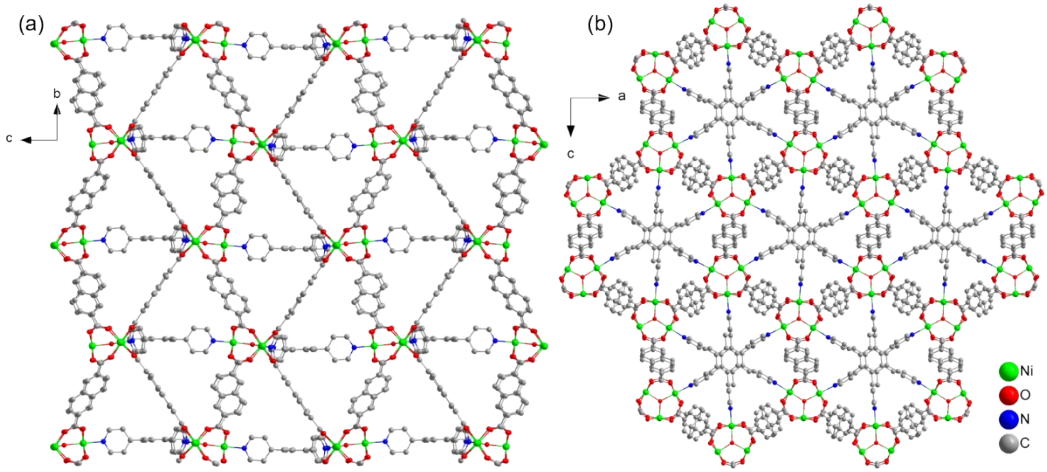

Fig. S4. A three-dimensional schematic diagram of the framework along the a-axis direction (a) and the b-axis direction (b).

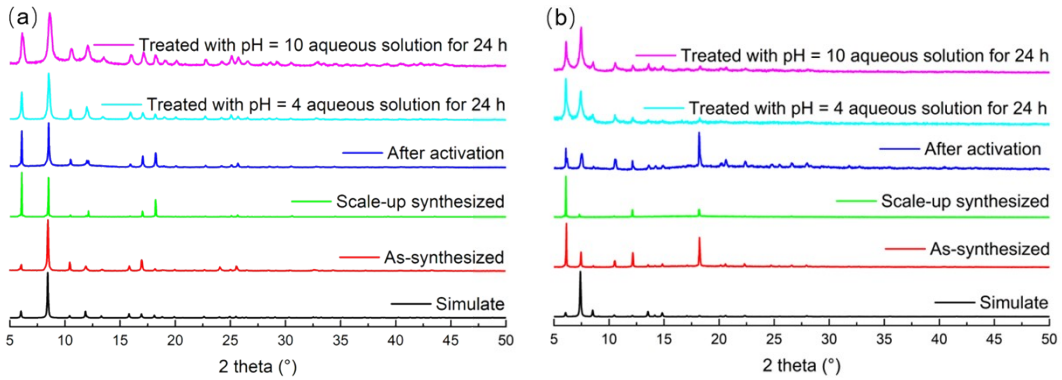

Fig. S5. PXRD patterns of as-synthesized and treated (a) DZU-72, (b) DZU-73.

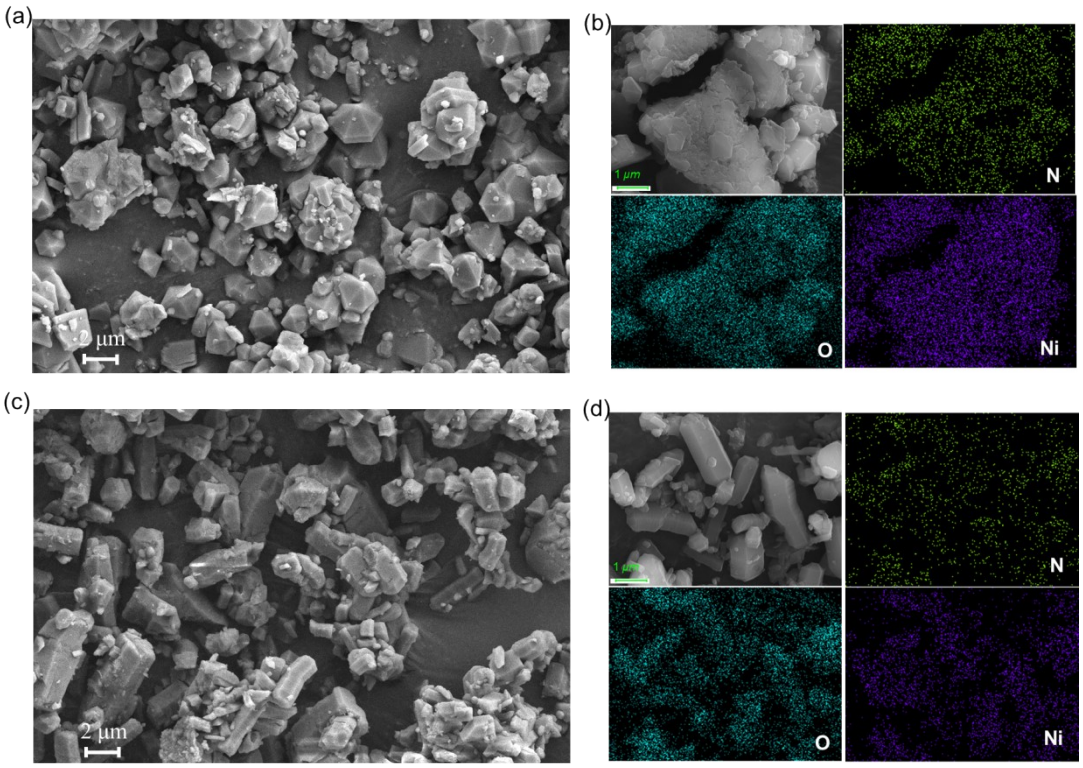

Fig. S6. SEM images of bulk-scale (a) DZU-72 and (b) DZU-73, and elemental mappings of (b) DZU-72 and (d) DZU-73 synthesized by stirring.

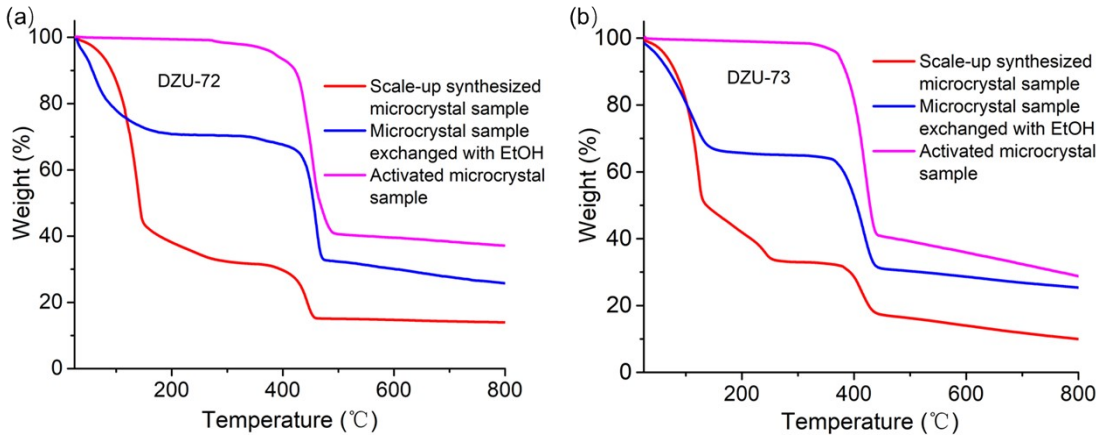

Fig. S7. TGA curves of two MOFs (a) DZU-72, and (b) DZU-73.

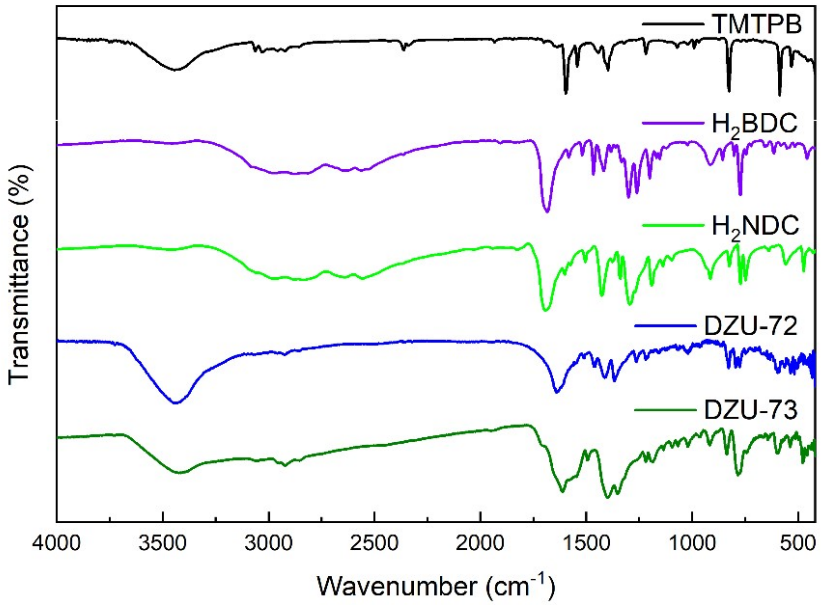

Fig. S8. FT-IR spectra of TMTPB, H_2BDC, H_2NDC ligands, and two MOFs.

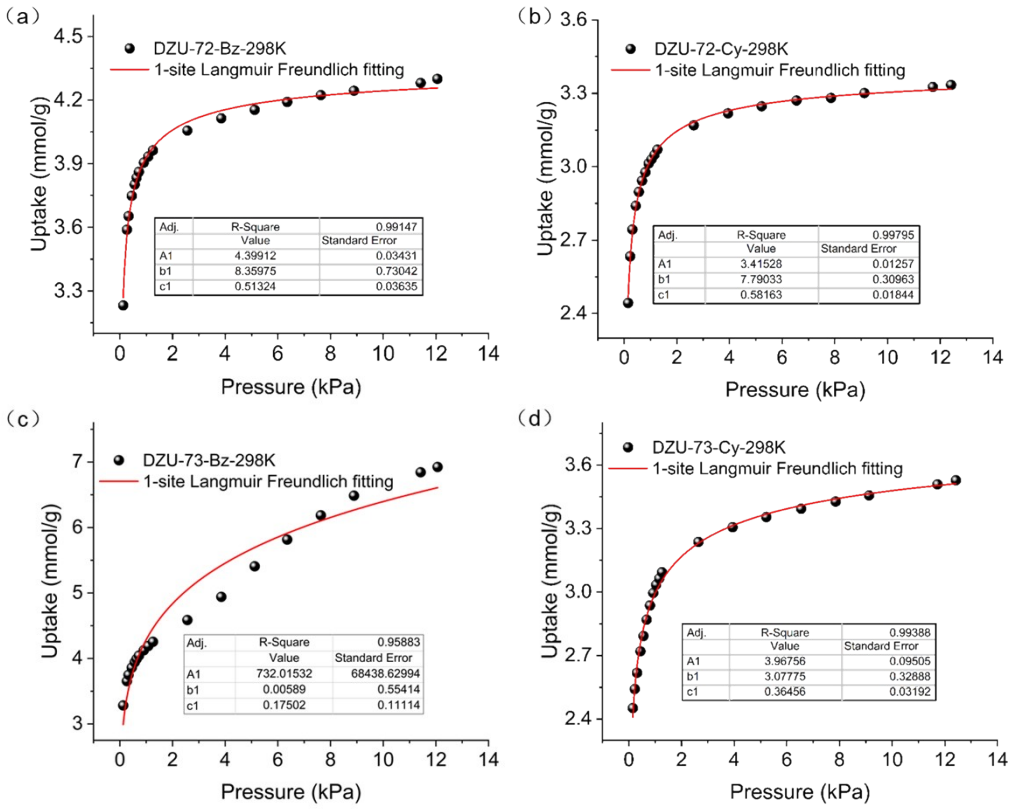

Fig. S9. Single-site Langmuir-Freundlich fitting (red lines) of (a, c) Bz and (b, d) Cy adsorption isotherms (black points) on DZU-72, and DZU-73 at 298 K.

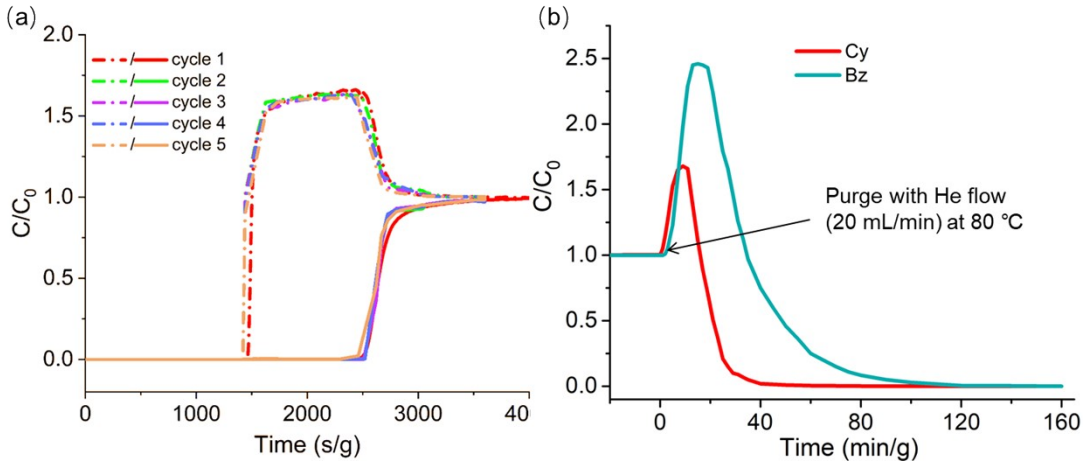

Fig. S10. (a) Five-cycle breakthrough curve of Bz/Cy in DZU-73. (b) The Bz and Cy desorption curves recorded on the column at 80 ℃ under He flow of 20 mL min^{-1}.

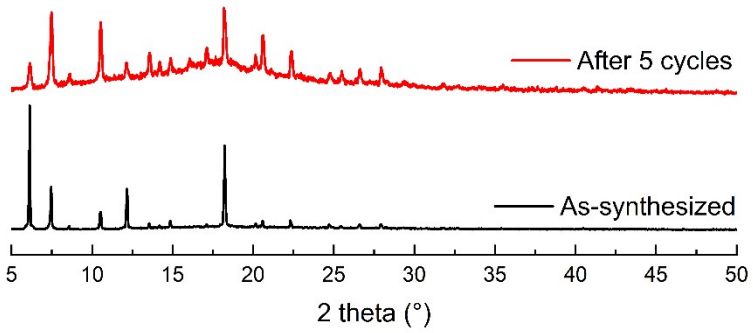

Fig. S11. PXRD pattern after cyclic test.

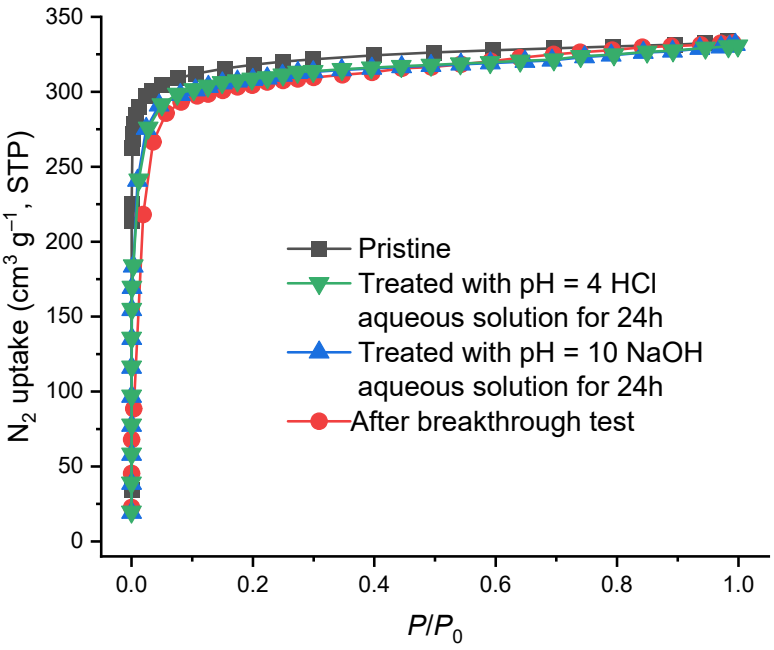

Fig. S12. 77 K N_2 adsorption isotherms of DZU-73 and its samples treated in different conditions, respectively.

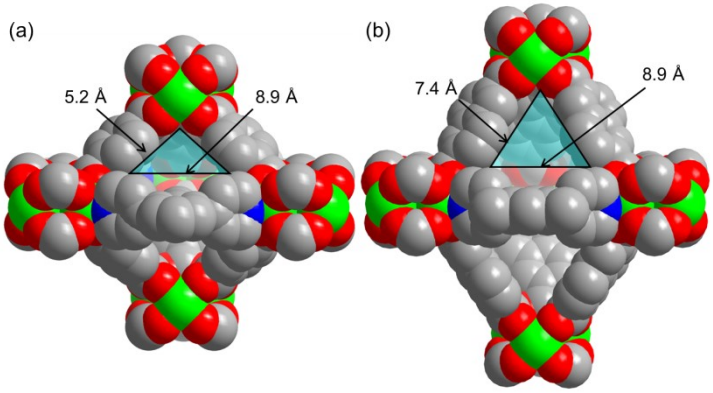

Fig. S13. Pore window size of cage B in (a) DZU-72, and (b) DZU-73.

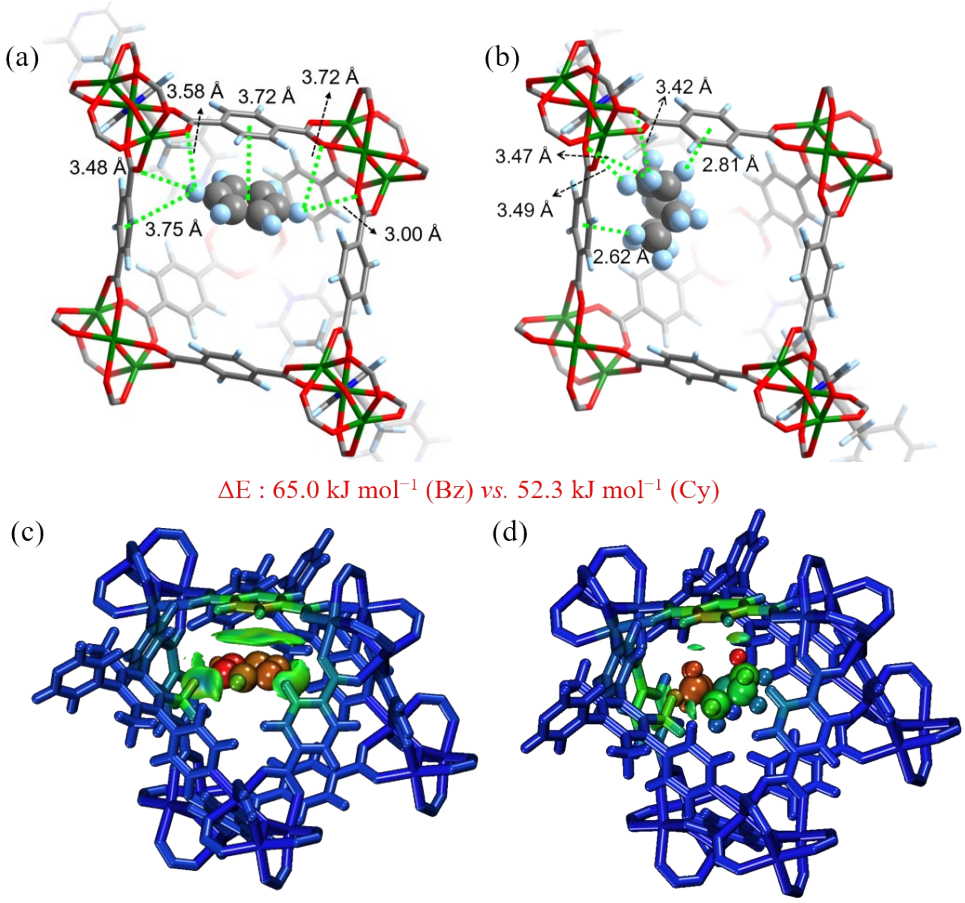

Fig. S14. Preferred binding sites for (a) Bz, and (b) Cy in DZU-72 as identified by DFT calculations (the close contact distances of Bz and Cy with the framework are indicated by green dashed lines). IGM analysis of (c) Bz and (d) Cy adsorption in DZU-72, where the green isosurface represents the vdW-type interaction region, and the red, green, and blue atoms of the MOF and gas molecules represent significant, moderate, and negligible contributions to the host-guest interactions, respectively.

Section 5. Additional Tables

Table S1. Crystal data and structure refinements of DZU-72 and DZU-73.

	DZU-72	DZU-73
Empirical formula	$C_{48}H_{34}N_3O_{13}Ni_3$	$C_{60}H_{40}N_3O_{13}Ni_3$
Formula weight	1035.88	1186.07
Radiation	MoKα	MoKα
Temperature (K)	150	150
Crystal system	hexagonal	orthorhombic
Space group	*P6₃/mmc*	$P2_12_12_1$
a (Å)	16.9190 (15)	20.718 (2)
b (Å)	16.9190 (5)	29.047 (3)
c (Å)	14.841 (3)	16.8737 (18)
α (°)	90	90
β (°)	90	90
γ (°)	120	90
V (Å^3)	3679.1 (10)	10154.6 (19)
Z	2	4
D_c (g cm^{-3})	0.916	0.750
F (000)	1018.0	2277.0
2*θ* range for data collection (°)	4.816 to 55.048	3.7 to 55.02
Goodness-of-fit on F^2	1.072	1.032
Final R indexes [I> = 2σ (I)]	$R_1 = 0.0614$, $wR_2 = 0.1782$	$R_1 = 0.0527$, $wR_2 = 0.1287$
Final R indexes [all data]	$R_1 = 0.0679$, $wR_2 = 0.1879$	$R_1 = 0.0680$, $wR_2 = 0.1358$
Largest difference in peak and hole (e Å^{-3})	1.69/-1.27	1.58/-0.59

The Alert level B in DZU-73_R checkcif file:

```
Alert level B
PLAT430_ALERT_2_B Short Inter D...A Contact  O5       ..N2       .       2.76 Ang.
                                    1-x,-1/2+y,3/2-z  =      3_646 Check
```

Answer: The dense accumulaiton of the ligand moleculars in the DZU-73 crystal structure trrggers this alert B.

Table S2. Summary of adsorption capacity and selectivity of some representative MOFs for Bz and Cy (298 K, P/P_0=1)

Sample	Bz uptake (mmol g^{-1})	Cy uptake (mmol g^{-1})	S_{BC}	Ref.
DZU-73	6.92	3.53	28.2	This work
DZU-72	4.30	3.33	11.5	This work
Zn-TCNQ-bpy	3.6	0.9	30	[48]
ZnL	5.6	1.1	4	[49]
Mn-TCNQ-bpy	3.7	1.7	16	[50]
Ni-ina-bdc	2.9	0.02	21	[52]
DAT-MOF-1	1.51	0.18	150	[53]
Cd-ATAIA	2.36	0.35	2.8	[54]
CBU-5	7.6	6	4	[55]

Table S3. Multi-constituent Adsorption Breakthrough Result of DZU-72.

Composition	Parameter	Unit	Breakthrough Point	Half Dry Point	Dry Point
Benzene	Time	s	2292.5	2833.9	5362.9
		s/g	2552.6	3155.5	5971.4
	Flow rates the outlet	V/V ％	0.311	2.913	5.504
	Adsorption capacity	ml/min (STP)	0.060	0.570	1.100
	Adsorption rate	mmol/g	2.202	2.562	3.051
Cyclohexane	Time	s	1246.8	1328.4	1521.2
		s/g	1388.2	1479.1	1693.8
	Flow rates the outlet	V/V ％	0.331	3.066	5.621
	Adsorption capacity	ml/min (STP)	0.059	0.560	1.054
	Adsorption rate	mmol/g	1.218	1.277	1.326

Composition	Saturated Adsorption Capacity (mmol/g)	Separation rate of Benzene to Cyclohexane
Benzene	3.088	2.8656
Cyclohexane	1.096	

Composition	Outflow Time	Delay Time	Bed Thickness	Diffusion Coefficient
Benzene	2210.93	988.27	6.2	0.0065
Cyclohexane	1224.53	104.22	6.2	0.0615

Table S4. Multi-constituent Adsorption Breakthrough Result of DZU-73.

Composition	Parameter	Unit	Breakthrough Point	Half Dry Point	Dry Point
Benzene	Time	s	2030.8	2123.0	2510.8
		s/g	2528.1	2642.8	3125.6
	Flow rates the outlet	V/V ％	0.314	2.919	5.501
	Adsorption capacity	ml/min (STP)	0.062	0.578	1.100
	Adsorption rate	mmol/g	2.180	2.253	2.315
Cyclohexane	Time	s	1182.2	1194.9	1207.6
		s/g	1471.6	1487.4	1503.3
	Flow rates the outlet	V/V ％	0.638	3.316	6.029
	Adsorption capacity	ml/min (STP)	0.114	0.607	1.136
	Adsorption rate	mmol/g	1.292	1.301	1.304

Composition	Saturated Adsorption Capacity (mmol/g)	Separation rate of Benzene to Cyclohexane
Benzene	2.335	3.2311
Cyclohexane	0.735	

Composition	Outflow Time	Delay Time	Bed Thickness	Diffusion Coefficient
Benzene	1360.15	804.12	5.2	0.0056
Cyclohexane	1169.44	502.65	5.2	0.0090

Section 6. References

[S1] Oxford Diffraction, CrysAlis Pro software. **2010**, Ver. 1.171.34, Yarnton, Oxfordshire. Oxford Diffraction Ltd.

[S2] G. M. Sheldrick, A short history of SHELX, *Acta crystallographica. Section A, Foundations of crystallography*, 2008, **64**, 112-122.

[S3] B. Rees, L. Jenner and M. Yusupov, Bulk-solvent correction in large macromolecular structures, *Acta Cryst. D,* 2005, **61**, 1299-1301.

[S4] Y.-Z. Zhang, X.-J. Kong, W.-F. Zhou, C.-H. Li, H. Hu, H. Hou, Z. Liu, L. Geng, H. Huang, X. Zhang, D.-S. Zhang and J.-R. Li, Pore Environment Optimization of Microporous Metal–Organic Frameworks with Huddled Pyrazine Pillars for C_2H_2/CO_2 Separation*, ACS Appl. Mater. Interfaces*, 2023, **15**, 4208-4215.

[S5] J. VandeVondele, M. Krack, F. Mohamed, M. Parrinello, T. Chassaing and J. Hutter, Quickstep: Fast and accurate density functional calculations using a mixed Gaussian and plane waves approach, *Comput. Phys. Commun.*, 2005, **167**, 103-128.

[S6] S. Goedecker, M. Teter and J. Hutter, Separable dual-space Gaussian pseudopotentials, *Phys. Rev. B*, 1996, **54**, 1703-1710.

[S7] C. Hartwigsen, S. Goedecker and J. Hutter, Relativistic separable dual-space Gaussian pseudopotentials from H to Rn, *Phys. Rev. B*, 1998, **58**, 3641-3662.

[S8] M. Krack and M. Parrinello, All-electron ab-initio molecular dynamics, *Phys. Chem. Chem. Phys.*, 2000, **2**, 2105-2112.

[S9] J. VandeVondele and J. Hutter, Gaussian basis sets for accurate calculations on molecular systems in gas and condensed phases, *J. Chem. Phys.*, 2007, **127**, 114105.

[S10] J. P. Perdew, K. Burke and M. Ernzerhof, Generalized Gradient Approximation Made Simple, *Phys. Rev. Lett.*, 1996, **77**, 3865-3868.

[S11] S. Grimme, J. Antony, S. Ehrlich and H. Krieg, A consistent and accurate ab initio parametrization of density functional dispersion correction (DFT-D) for the 94 elements H-Pu, *J. Chem. Phys.*, 2010, **132**, 154104.

[S12] C. Lefebvre, G. Rubez, H. Khartabil, J.-C. Boisson, J. Contreras-García and E. Hénon, Accurately extracting the signature of intermolecular interactions present in the NCI plot of the reduced density gradient versus electron density, *Phys. Chem. Chem. Phys.*, 2017, **19**, 17928-17936.

[S13] T. Lu and F. Chen, Multiwfn: A multifunctional wavefunction analyzer, *J. Comput. Chem.*, 2012, **33**, 580-592.

[S14] W. Humphrey, A. Dalke and K. Schulten, VMD: Visual molecular dynamics, *J. Mol. Graph. Model.*, 1996, **14**, 33-38.